DYNAMIC FLUID FLOW IN HETEROGENEOUS POROUS MEDIA AND THROUGH A SINGLE FRACTURE WITH ROUGH SURFACES

by

Xiaomin Zhao, C.H. Cheng, Xiaoming Tang*, and M. Nafi Toksöz

Earth Resources Laboratory
Department of Earth, Atmospheric, and Planetary Sciences
Massachusetts Institute of Technology
Cambridge, MA 02139

***NER Geoscience**
1100 Crown Colony Drive
Quincy, MA 02169

ABSTRACT

This study investigates the frequency-dependence of fluid flow in heterogeneous porous media using the theory of dynamic permeability and a finite-difference method. Given a permeability distribution, the dynamic permeability is applied locally to calculate the frequency-dependence of fluid flow at each local point. An iterative Alternating Direction Implicit finite-difference technique is applied to calculate the flow field in the frequency domain. We compare the flow through a 2-D heterogeneous porous medium and that through an equivalent homogeneous medium and find that the two media do not behave equivalently as a function of frequency. At very low-frequencies, the heterogeneous medium is less conductive than the homogeneous medium, However, in the transition region from quasi-static to dynamic regimes, the former medium becomes more conductive than the latter medium, with the ratio of the former flow over the latter flow reaching a maximum in this region. The larger the scale, or the higher the degree of the heterogeneity, the higher this maximum is. This finding is important for studying the interaction of a borehole stoneley wave with a heterogeneous porous formation.

The finite-difference technique is also applied to simulate frequency-dependent flow through a single fracture with rough surfaces. It is shown that the flow exhibits strong frequency-dependence even for small fractures with contacting surfaces. The amount of flow through the fracture is reduced by the surface roughness .

INTRODUCTION

Fluid flow in porous media is an important topic in the study of flow of oil or gas in petroleum reservoirs. In many applications where the fluid driven (pressure) source is time invariant, steady-state (time-independent) flow is assumed and the flow can be modeled for any distribution of heterogeneous porous media using a finite-difference technique (Zhao and Toksöz, 1991). When the fluid driven source changes moderately with time, such as the pressure transient tests in a borehole (Melville et al, 1991) and in laboratory measurements (Brace et al, 1968; Kamath et al., 1990; Bernabé, 1991), fluid flow can be modeled as a diffusion process in which the fluid transport properties such as permeability are still regarded as independent of time (or frequency) (Zhao and Toksöz, this volume). Moreover, in applications related to wave propagation, such as vertical seismic profiling and acoustic logging, fluid flow associated with the pressure disturbance set up by seismic wave propagation is dynamic in nature and may strongly depend on frequency. In fact, in these situations, the frequency-dependent flow becomes the Biot's slow wave (Biot, 1956a,b) in a porous medium.

To characterize the frequency-dependent fluid transport property, Johnson et al. (1987) developed the theory of dynamic permeability. Applying the concept of dynamic permeability to the problem of acoustic logging in permeable porous formations, Tang et al. (1991) showed that the dynamic permeability captures the frequency-dependent behavior of Biot's slow wave and correctly predicts the effects of formation permeability on borehole Stoneley waves. The theory of dynamic permeability is formulated assuming the homogeneity of the porous medium. The natural geological medium, however, contains heterogeneities of various scales. It would be interesting to apply the dynamic permeability to the heterogeneous porous media to study the overall behavior of fluid flow through the media. In this study, we will model the dynamic fluid flow in the heterogeneous porous media using the theory of dynamic permeability. A finite-difference method will be developed to model the effects of heterogeneities.

A problem that has attracted much research interest is fluid flow through a rough-walled fracture or joint. Brown (1987, 1989) and Zimmerman et al. (1991) have modeled the steady-state fluid flow through the fracture and showed that the roughness of the fracture surfaces significantly affects the fluid flow when the surfaces are in contact. In the characterization of borehole fractures using acoustic logging (Paillet et al., 1989; Hornby et al., 1989), the response of the fracture to the dynamic pressure set up by the logging waves is important for characterizing the fracture permeability. In this situation, fluid flow in fractures is dynamic in nature. Tang and Cheng (1989) have studied the dynamic flow through a plane fracture bounded by two parallel walls. Natural fracture surfaces, however, exhibit roughness (Brown, 1987). It is important to understand the effects of surface roughness on the dynamic fluid flow in order to correctly model the dynamic response of natural fractures to borehole acoustic waves. Tang et al. (1991)

have shown that the theory of dynamic permeability, when applied to the parallel-wall fracture, is equivalent to the theory of fracture dynamic conductivity. Therefore, if we assume that the dynamic permeability for a parallel-wall fracture holds locally in a fracture, then we can use the finite-difference code developed for heterogeneous porous media to model the dynamic flow in a rough-walled fracture.

In the following, we first discuss the theory of dynamic permeability and governing equations for the dynamic fluid flow. Then we develop a finite-difference technique to solve the flow equation in the frequency domain. Finally, we apply the finite-difference technique to study the dynamic flow through a single fracture with rough surfaces.

THEORY

The equation that describes the time-dependent pressure disturbance P in a porous medium is

$$\nabla \cdot (\alpha \nabla P) = \frac{\partial P}{\partial t} \ , \tag{1}$$

where α is the fluid diffusivity:

$$\alpha = \frac{k\kappa_f}{\phi\mu} \tag{2}$$

with k = permeability, κ_f = fluid incompressibility, ϕ = porosity, and μ = fluid viscosity. We Fourier-transform Eq. (1) into the frequency domain and modify the fluid diffusivity (Eq. 2) by replacing the permeability k with Johnson et al.'s (1987) dynamic permeability and introducing a correction ξ for solid compressibility (Tang et al., 1991):

$$\alpha(\omega) = \frac{k(\omega)\kappa_f}{\phi\mu(1+\xi)} \ . \tag{3}$$

We then have

$$\nabla \cdot [\alpha(\omega) \nabla P] + i\omega P = 0 \ . \tag{4}$$

In the present study, we neglect the effects of solid compressibility by assuming that the fluid compressibility is much greater than that of the solid, i.e., $\xi \sim 0$. The functional form of dynamic permeability is given by (Johnson, et al., 1987)

$$k(\omega) = \frac{k_0}{\left(1 - \frac{i}{\beta}\tau k_0 \rho_0 \omega / \mu\phi\right)^{\frac{1}{2}} - i\frac{\tau k_0 \rho_0 \omega}{\mu\phi}} \ , \tag{5}$$

where k_0 is the conventional Darcy permeability which is independent of frequency, τ is the tortuosity of the porous medium, ρ_0 is fluid density, and ω is angular frequency, and $\beta = 2$ is for a porous medium and $\beta = 3$ is for a fracture. Based on the frequency dependence of $k(\omega)$, it can be shown (Tang et al., 1991) that Eq. (4) describes a diffusive fluid

motion at low frequencies. At high frequencies, this motion becomes a propagational wave. Therefore, Eq. (4) describes Biot's (1956a, b) slow wave in a porous medium with an incompressible solid matrix.

In this study, we will investigate the behavior of flow field over a distribution of two-dimensional (2-D) heterogeneities. To model the effects of the 2-D heterogeneities on the fluid flow, we assign a 2-D distribution for the permeability k_0, i.e.,

$$k_0 = k_0(x, y) \quad . \tag{6}$$

In this way, the dynamic permeability (Eq. 5) is not only a function of frequency, but also a function of the spatial coordinates x and y. Because of the spatial variation of k_0, flow in the heterogeneous porous medium may exhibit different characteristics at different locations. For example, in regions where k_0 is small, the flow is dominated by viscous diffusion, whereas in regions where k_0 is high, dynamic effects may become significant and the flow becomes a propagational wave. Because $k(\omega; x, y)$, as well as $\alpha(\omega)$, change spatially, Eq. (4) is written as

$$\frac{\partial}{\partial x}\left[\alpha(\omega; x, y)\frac{\partial P}{\partial x}\right] + \frac{\partial}{\partial y}\left[\alpha(\omega; x, y)\frac{\partial P}{\partial y}\right] + i\omega P = 0 \quad . \tag{7}$$

This equation, together with given boundary conditions, describes the fluid pressure fields in the 2-D heterogeneous porous medium for the given frequency ω. We choose to model the dynamic flow in the frequency domain because the dynamic permeability is defined as the function of frequency. This formulation allows us to study the flow behavior over different frequency ranges.

FINITE-DIFFERENCE MODELING

For the finite-difference modeling, it is convenient to use dimensionless variables. We introduce the dimensionless permeability k' and spatial variables x' and y' as follows:

$$\begin{aligned} k_0(x, y) &= k_{max} k'(x, y) \qquad 0 < k' < 1 \\ x &= L_x x' \qquad 0 < x' < 1 \\ y &= L_y y' \qquad 0 < y' < 1 \end{aligned}$$

where k_{max} is the maximum permeability over the region of interest, x' and y' are the dimensionless variables in x and y directions, respectively. For a square 2-D grid, we assume $L_x = L_y = L$. We also introduce the characteristic frequency of the model

$$\omega_0 = \frac{\kappa_f k_{max}}{\phi \mu L^2} \quad . \tag{8}$$

The dimensionless frequency Ω is defined as

$$\Omega = \frac{\omega}{\omega_0} \ . \tag{9}$$

Using the dimensionless variables, Eq. (7) becomes

$$\frac{\partial}{\partial x'}\left[A(\omega;x',y')\frac{\partial P}{\partial x'}\right] + \frac{\partial}{\partial y'}\left[A(\omega;x',y')\frac{\partial P}{\partial y'}\right] + i\Omega P = 0 \ , \tag{10}$$

where the dimensionless dynamic permeability is

$$A(\omega;x',y') = \frac{k'(x',y')}{\left(1-\frac{i}{2}\tau k_{max}k'(x',y')\frac{\rho_0\omega}{\mu\phi}\right)^{1/2} - i\tau k_{max}k'(x',y')\frac{\rho_0\omega}{\mu\phi}} \ . \tag{11}$$

It is interesting to note that, because the spatial variation of $k'(x',y')$ in $A(\omega;x',y')$ is coupled with the frequency ω, $A(\omega;x',y')$ may have different distributions over the 2-D grids x' and y' at different frequencies.

Forward difference solution of Eq. (10) (which is a Helmholtz type equation) is unstable, especially for large Ω values where the dynamic effects become significant. This can be shown by analyzing a 1-D Helmholtz equation

$$\frac{d^2P}{dx^2} + \lambda^2 P = 0 \ . \tag{12}$$

Substituting $P = P_0 e^{i\lambda m x}$ (where $x = m\Delta x$, $m = 0, 1, 2, \cdots, M$) into Eq. (12) and using the forward difference $\frac{d^2P}{d^2x} = \frac{P_{m+1} - 2P_m + P_{m-1}}{\Delta x^2}$, we have the following stability equation:

$$\sin^2\left(\frac{\lambda\Delta x}{2}\right) = \left(\frac{\lambda\Delta x}{2}\right)^2 \ . \tag{13}$$

This equation holds only when $\lambda\Delta x$ is small. In Eq. (13), however, $\lambda = \sqrt{i\Omega}$ is big when Ω is big, Eq. (12) cannot have a solution unless Δx is exceedingly small. We therefore use an iterative procedure to solve Eq. (10). We write Eq. (10) as

$$\frac{\partial}{\partial x'}\left[A(\omega;x',y')\frac{\partial P}{\partial x'}\right] + \frac{\partial}{\partial y'}\left[A(\omega;x',y')\frac{\partial P}{\partial y'}\right] + i\Omega P = \frac{\partial P}{\partial t'} \ , \tag{14}$$

where t' is a dimensionless time. The steady-state solution of Eq. (14) will be the solution of Eq. (10), and the solution of Eq. (14) will be unconditionally stable if we solve it using the Alternating Direction Implicit (ADI) scheme (Ferziger, 1981; Zhao and Toksöz, this volume). Using the ADI method, the finite-difference form of Eq. (14) is

$$\begin{aligned} -\mu_1 B_{i,j} P_{i-1,j}^{n+\frac{1}{2}} + [1 + \mu_1(B_{i,j} + B_{i+1,j} - i\Omega\Delta x^2)]P_{i,j}^{n+\frac{1}{2}} - \mu_1 B_{i+1,j} P_{i+1,j}^{n+\frac{1}{2}} \\ = \mu_2 C_{i,j} P_{i,j-1}^{n} + [1 - \mu_2(C_{i,j} + C_{i,j+1})]P_{i,j}^{n} \mu_2 C_{i,j+1} P_{i,j+1}^{n} \end{aligned} \tag{15}$$

$$-\mu_2 C_{i,j} P_{i,j-1}^{n+1} + [1 + \mu_2(C_{i,j} + C_{i,j+1})] P_{i,j}^{n+1} - \mu_2 C_{i,j+1} P_{i,j+1}^{n+1}$$
$$= \mu_1 B_{i,j} P_{i-1,j}^{n+\frac{1}{2}} + [1 - \mu_1(B_{i,j} - B_{i+1,j} - i\Omega\Delta x^2)] P_{i,j}^{n+\frac{1}{2}} + \mu_1 B_{i+1,j} P_{i+1,j}^{n+\frac{1}{2}} \quad (16)$$

where,

$$\mu_1 = \frac{\Delta t'}{2\Delta x'^2}$$
$$\mu_2 = \frac{\Delta t'}{2\Delta y'^2}$$

and

$$B_{i,j} = \sqrt{A_{i,j} * A_{i+1,j}}$$
$$C_{i,j} = \sqrt{A_{i,j} * A_{i,j+1}} \ .$$

Here we use the geometric average for the mid-point between two adjacent grids because it gives a better approximation for the point when the values on the two adjacent grids differ by orders. The boundary conditions are specified by assigning no-flow conditions for $y' = 0$ and $y' = 1$, i.e.,

$$\frac{\partial P'}{\partial y'} = 0 \qquad \text{at } y' = 0 \text{ and } y' = 1 \ . \quad (17)$$

The pressure spectrum $P_0(\omega)$ is assigned to the $x' = 0$ boundary. At $x' = 1$, the pressure is set to zero. With the algorithm, the solution is iterated with increasing n. The solution to Eq. (10) is obtained when the difference between P^{n+1} and P^n is sufficiently small.

TESTING THE FINITE-DIFFERENCE ALGORITHM

As a test of the numerical algorithm, we compare the finite-difference results with the results from the analytical solution for a simple 1-D case Eq. (12). For the 1-D case, if we assign $P|_{x=0} = P_0$ and $P|_{x=L} = 0$, then the solution is

$$P(\omega; x) = P_0 \frac{\sin[\lambda(L - x)]}{\sin \lambda L} \ , \quad (18)$$

where λ now equals $\sqrt{\frac{i\omega\phi\mu}{k(\omega)\kappa_f}}$ for the dynamic flow problem. Figure 1 shows the comparison between the results of the finite-difference algorithm and Eq. (18), where the amplitude, the real and imaginary parts of the pressure spectrum $P(\omega; x)$ are plotted.

The parameters are $k_0 = 1$ Darcy, $\phi = 0.2$, $\kappa = 2.25 \times 10^9$ Pa, and $\mu = 1.14 \times 10^3$ Pa-s. For the finite-difference scheme, the pressure along the middle line $y' = L/2$ is used. The two results are in almost exact agreement (the no-flow boundary condition at $y' = 0$ and $y' = 1$ makes the 2-D solution very close to the 1-D solution). The behavior of the dynamic flow pressure versus distance is also demonstrated in Figures 1 (a) through (c) for frequency = 100 Hz, 5000 Hz, and 20000 Hz cases. At low frequencies, the pressure $\sim x$ relation is a linear function. As frequency increases the pressure decreases and becomes oscillatory, showing that the flow becomes a propagational wave and decays rapidly with distance.

RESULTS FOR HETEROGENEOUS MEDIA

In Figure 2, we show two heterogeneous distributions generated by Gaussian (a) and von-Karman (b) correlation functions and the finite-difference modeling results for the two distributions. The von-Karman distribution has a fractal dimension of $D = 2.5$ at small wavelengths (Frankel and Clayton, 1986), and thus it is much rougher than the Gaussian distribution. In spite of the roughness, the fluid pressures for the two distributions are almost the same (Figure 2c and d for frequency = 1000 and 30000 Hz, respectively), showing that the dynamic flow is not sensitive to the roughness of the heterogeneities as long as the wavelength is greater than the small scale roughness. This is also true for the steady-state flow (Zhao and Toksöz, 1991) and transient flow (Zhao and Toksöz, this volume) cases.

To study the behavior of the heterogeneous porous medium in conducting the dynamic flow, we compute the flow rate q_x into the medium at the $x = 0$ boundary, as

$$q_x = \frac{1}{L_y} \int_0^{L_y} \left\{ \frac{k(x,y)}{\mu} \frac{\partial P}{\partial x} \right\} \Big|_{x=0} dy \ . \tag{19}$$

In the logging situation, this flow corresponds to the dynamic flow into a formation due to the pressure disturbance of the borehole waves. In the effective medium approach, a heterogeneous medium having random variations is often treated as an equivalent homogeneous medium whose property (i.e., permeability in the present study) is the average property of the heterogeneous medium. We have calculated the flow rate for the heterogeneous medium (generated by Gaussian correlation function) and the homogeneous medium as a function of frequency using the same parameters as those used in Figure 1. In Figure 3, we plot the ratio q_{hete}/q_{homo} versus frequency for different correlation lengths ($a = 3$, 5, and 10, the model length is 64). Here q is the amplitude of the complex flow rate of Eq. (19). If the behavior of the heterogeneous medium is the same as that of the equivalent homogeneous medium, the ratio q_{hete}/q_{homo} would plot as a horizontal line of height 1. However, this ratio demonstrates a strong frequency-dependent behavior. At very low frequencies, q_{hete}/q_{homo} is always less than 1. As

frequency increases, this ratio increases to reach a maximum. At very high frequencies, this ratio approachs a constant. The maximum lies within the transition region between the quasi-static and dynamic regimes and reflects the complexity of dynamic flow in heterogeneous media. The variation of q_{hete}/q_{homo} is also a function of the scale of the heterogeneities. This scale is governed by the correlation length a of the medium. As a increases the range of variation also increases. For example, the curve in Figure 3 for the $a = 10$ case varies by more than 30% from zero frequency to the maximum, while for $a = 3$, this range is reduced about 10%. It can be concluded that when the correlation length is very small, the heterogeneous medium will behave like an equivalent homogeneous medium.

Th above results may have important implications to Stoneley wave logging in a heterogeneous formation. For an average permeability of 1 Darcy, the maximum of the flow ratio is around 5 kHz, within the frequency of Stoneley wave measurements. In addition, the borehole diameter is generally on the order of 0.2 m and is in many cases comparable to the scale of formation heterogeneities. When the q_{hete}/q_{homo} maximum lies within the frequency range of the measurements, more flow will be conducted into a heterogeneous formation than into a homogeneous formation. It is therefore expected that the flow into the heterogeneous formation may significantly affect the Stoneley wave propagation in this formation.

DYNAMIC FLUID FLOW THROUGH A SINGLE FRACTURE WITH ROUGH SURFACES

We now apply the finite-difference formulation for heterogeneous media to study the dynamic flow in a single fracture with rough surfaces. The roughness of a natural rock surface has power spectra of the form $G(\Lambda) \sim \left(\frac{2\pi}{\Lambda}\right)^{-(7-2D)}$ (Brown, 1987), where Λ is the wavelength, and D is the fractal dimension of the surface and falls in the range $2.0 \leq D \leq 2.5$. For this study, the fractal model is assumed to adequately describe the character of rock fractal surfaces. To form a fracture, two surfaces with the same fractal dimension of $D = 2.5$, but generated with different sets of random numbers, were placed together (with one of them flipped over) at some fixed distance d_m between the mean planes of the two surfaces. Figure 4 shows the two surfaces. The local distance between the two surfaces gives the aperture distribution $d(x, y)$. The model surfaces are generated using Gaussian random distribution with a standard deviation σ and a von-Karman correlation function having a fractal dimension $D = 2.5$. When $d_m = 4.24\sigma$, the two surfaces begin to contact each other. At the "contact", the local aperture $d(x, y)$ is set to zero assuming that the deformation of the contact is ignored (Brown, 1987). Figure 5 shows examples of the local aperture distribution generated with the two surfaces of Figure 4 at various d_m values [(a) $d_m = 10\sigma$, (b) $d_m = 3\sigma$, (c) $d_m = 1\sigma$]. For a rough-walled fracture, a measure of aperture in terms of fluid flow is the mean

aperture defined as (Brown, 1987)

$$\bar{d} = \frac{1}{L_x L_y} \int_0^{L_x} \int_0^{L_y} d(x,y) dx dy \ . \tag{20}$$

The mean aperture represents the aperture available to flow.

If we assume that $d(x,y)$ varies slowly in the plane of the fracture and that the permeability for a parallel plane fracture holds locally, we then have

$$k_0(x,y) = \frac{d^2(x,y)}{12} \ . \tag{21}$$

Eq. (21) gives the static (zero-frequency) permeability distribution over the fracture plane. Applying the dynamic permeability locally, we have

$$k(\omega;x,y) = \frac{d^2(x,y)/12}{(1 - i\omega\rho_0 d^2(x,y)/36\mu)^{1/2} - i\omega\rho_0 d^2(x,y)/12\mu} \tag{22}$$

where we have used $\tau = 1$ [straight flow at (x,y)] and $\phi = 1$ (aperture filled with fluid) in Eq. (5). Tang et al. (1991) showed that Eq. (22) agrees almost exactly with the theory of dynamic conductivity derived for a parallel wall fracture. With the dynamic permeability distribution specified for each (x,y) using Eq. (22), the finite-difference technique of the previous section is applied to calculate the dynamic fluid flow over the 2-D grids for various frequencies and separations d_m/σ. The results are presented in the following section.

Numerical Results and Comparison with the Parallel Plate Model

For dynamic fluid flow through a rough-walled fracture, the measurable quantity is the average flow rate per unit fracture length into the fracture opening:

$$\bar{q} = \frac{1}{L_y} \int_0^{L_y} \left\{ d(x,y) \frac{k(\omega,x,y)}{\mu} \frac{\partial P}{\partial x} \right\} \Big|_{x=0} dy \ , \tag{23}$$

where $k(\omega,x,y)|_{x=0}$ is the fracture dynamic permeability of Eq. (22) evaluated at $x = 0$. In the borehole situation, the average flow rate $\bar{q}$ represents the dynamic flow into a borehole fracture due to the acoustic wave excitation in the borehole.

For the finite-difference modeling, we set $L_x = L_y = L = 0.2$m, the standard deviation $\sigma \approx 1.6\mu$m. The flow field through the fracture is computed at increasing frequency with d_m/σ equal to various values. The dynamic effects of the fluid motion are controlled by the thickness of viscous skin depth $\delta = \sqrt{\frac{2\mu}{\rho\omega}}$ compared to the fracture aperture $\bar{d}$ (Johnson et al., 1987; Tang and Cheng, 1989). For water ($\mu = 1.14 \times 10^{-3}$

Pa s), δ is 19.05 μm at 1000 Hz and 3.48 μm at 30000 Hz. The two surfaces will begin to contact at about $4.26\sigma = 6.8$ μm. By varying d_m/σ and frequency, fluid flow in a rough-walled fracture can be simulated for quasi-static as well as dynamic regimes. For each simulated pressure field, the pressure gradient at $x = 0$ is calculated and used in Eq. (23) to compute the flow rate. For comparison with the parallel plate model, we compute the dynamic flow rate into a plane fracture using the dynamic fracture conductivity $\bar{c}(\omega, \bar{d})$ (Tang and Cheng, 1989)

$$\vec{q} = \bar{c}(\omega, \bar{d}) \bigtriangledown P \ . \tag{24}$$

Assuming a 1-D flow field along a fracture of length L, the pressure in the fracture is given in Eq. (18). We then have

$$\frac{\partial P}{\partial x}|_{x=0} = P_0(\omega)\lambda \frac{\cos \lambda L}{\sin \lambda L} \ . \tag{25}$$

In addition, the dynamic conductivity in Eq. (24) is calculated using Eq. (12) of Tang and Cheng (1989) with $\bar{d}$ of Eq. (20) as the aperture of the equivalent plane fracture.

Before we compare the results versus frequency, we show the zero-frequency results calculated using the iterative finite-difference algorithm. The results are shown as q_{rough}/q_{plane} vs. d_m/σ in Figure 6, where q_{rough} is the calculated rough-wall flow rate and q_{plane} is the cubic law flow rate calculated using Eqs. (24) and (25) with $\omega = 0$, and with the plane fracture thickness equal to $\bar{d}$ of the rough-walled fracture. The ratio of the mean plane separation d_m over standard deviation of the roughness is the standardized separation between the mean planes of the two fracture surfaces. As shown in Figure 6, for small separations, q_{rough} is significantly reduced compared with q_{plane} because of the contacting of the rough surfaces. As d_m/σ increases to 10, q_{rough}/q_{plane} approaches 1. The overall behavior of q_{rough}/q_{plane} agrees with the results calculated by Brown (1987) for the steady flow case.

Next, we compare the results for $d_m/\sigma = 1$, 3, 6, and 10 and for frequencies ranging from 0 to 30000 Hz. Figure 7 shows the calculated rough-walled fracture flow rate q_{rough} (solid dots) and the parallel plane fracture flow rate q_{plane} (dashed curves) calculated using Eq. (18) with the plane fracture aperture equal to $\bar{d}$. As seen from Figure 7, the flow rate shows strong frequency dependence (or dynamic effects), increasing with increasing frequencies. Even for the very small fracture with contacting surfaces (e.g., $d_m/\sigma = 1$ case), the dynamic effect is still significant. The rough-wall fracture flow rate is smaller than that of the equivalent plane fracture. This difference demonstrates that the effect of the fracture surface roughness is to reduce the fluid flow in static as well as dynamic regimes. In the high-frequency dynamic regime, the ratio q_{rough}/q_{plane} increases to approach 1 as the fracture aperture increases. For example, at 30000 Hz, the ratio for $d_m/\sigma = 1$, 3, 6, and 10 are 0.66, 0.68, 0.82, and 0.92, respectively. The high-frequency results are analogous to the results of electrical current through a fracture

modeled by Brown (1989), because in both cases the local fracture conductivities of both the high-frequency fluid flow and electrical current are linearly proportional to the local aperture (see Brown, 1989 and Tang and Cheng, 1989).

CONCLUSIONS

In this study, we have developed a finite-difference algorithm for simulating dynamic fluid flow in the frequency domain for an arbitrarily heterogeneous porous media. A heterogeneous medium behaves differently than a homogeneous medium, especially at low to medium frequencies. At medium frequencies, the heterogeneous medium conduct more flow than the homogeneous one, depending on the scale of the heterogeneities. In the logging situation, since the formation may contain various heterogeneities, the heterogeneous flow behavior can cause the discrepancy between the field observation and the theoretical prediction from Biot's theory for a homogeneous medium.

Applying the finite-difference technique to study the dynamic fluid flow through a single fracture with rough surfaces, we have demonstrated the effects of surface roughness on the dynamic flow. For dynamic as well as steady flow cases, the surface roughness reduces the amount of fluid flow through the fracture in the static and dynamic regimes. When the separation between the two fracture surfaces is about 10 times the standard deviation of the roughness, the behavior of the fracture approaches that of a parallel plane fracture

The finite-difference technique developed here can find useful applications to the study of tube wave propagation in a heterogeneous porous formation. For example, by developing the frequency-dependent finite-difference algorithm in cylindrical coordinates, we can study the propagation of borehole Stoneley waves in relation to the dynamic fluid flow into a heterogeneous porous formation. We can also model the Stoneley wave reflection and transmission across a natural fracture zone having a heterogeneous permeability distribution.

ACKNOWLEDGEMENT

We thank Prof. L.W. Gelhar for his helpful discussion on the finite-difference algorithm. This research was supported by the Borehole Acoustics and Logging Consortium at M.I.T., and Department of Energy grant #DE-FG02-86ER13636.

REFERENCES

Bernabé, Y., 1991, On the measurement of permeability in anisotropic rocks, in *Fault Mechanism and Transport Properties of Rocks: A Festchrift in Honor of W.F. Brace* edited by B.J. Evans and T.F. Wong, in press, Academic Press, London.

Biot, M.A., 1956a, Theory of propagation of elastic waves in a fluid-saturated porous solid, I: Low frequency range, *J. Acoust. Soc. Am., 28*, 168–178.

Biot, M.A., 1956b, Theory of propagation of elastic waves in a fluid-saturated porous solid, II: Higher frequency range, *J. Acoust. Soc. Am., 28*, 179–191.

Brace, W.F., J.B. Walsh, and W.T. Frangos, 1968, Permeability of granite under high pressure, *J. Geophys. Res., 73*, 2225–2236.

Brown, S.R., 1987., Flow through rock joints: the effect of surface roughness, *J. Geophys. Res., 92*, 1337–1347

Brown, S.R., 1989, Transport of fluid and electric current through a single fracture, *J. Geophys. Res., 94*, 9429–9438.

Brown, S.R., and C.H. Scholz, 1985a, The closure of random elastic surfaces in contact, *J. Geophys. Res., 90*, 5531–5545.

Brown S.R., and C.H. Scholz, 1985b, Broad bandwidth study of the topography of natural rock surfaces, *J. Geophys. Res., 90*, 12575–12582.

Ferziger, J.H., 1981, *Numerical Methods for Engineering Applications*, John Wiley & Sons, Inc., New York.

Frankel, A., and R. Clayton, 1986, Finite difference simulations of seismic scattering: implications for the propagation of short-period seismic waves in the crust and models of crustal heterogeneity, *J. Geophys. Res., 91*, 6465–6489.

Hornby, B.E., D.L. Johnson, K.H. Winkler, and R.A. Plumb, 1989, Fracture evaluation using reflected Stoneley-wave arrivals, *Geophysics, 54*, 1274–1288.

Johnson, D.L., J. Koplik, and R. Dashen, 1987, Theory of dynamic permeability and tortuosity in fluid-saturated porous media, *J. Fluid Mech., 176*, 379–400.

Kamath, J, R.E. Boyer, and F.M. Nakagawa, 1990, Characterization of core scale heterogeneities using laboratory pressure transients, *Society of Petroleum Engineers*, 475–488.

Melville, J.G., F.J. Molz, O. Göven, and M.A. Widdowson, 1991, Multilevel slug tests with comparisons to tracer data, *Ground Water, 29*, 897–907.

Paillet, F.L., C.H. Cheng, and X.M. Tang, 1989, Theoretical models relating acoustic tube-wave attenuation to fracture permeability - reconciling model results with field data, *Trans., Soc. Prof. Well Log Analyst, 30th Ann. Symp.*

Tang, X.M., and C.H. Cheng, 1989, A dynamic model for fluid flow in open borehole fractures, *J. Geophys. Res., 94*, 7567–7576.

Tang, X.M., C.H. Cheng, and M.N. Toksöz, 1991, Dynamic permeability and borehole Stoneley waves: A simplified Biot-Rosenbaum model, *J. Acoust. Soc. Am., 90*, 1632–1646.

Zhao, X.M., and M.N. Toksöz, 1991, Permeability anisotropy in heterogeneous porous media, 61st SEG Ann. Mtg. Expanded Abstracts, 387–390

Zhao, X.M., and M.N. Toksöz, Transient fluid flow in heterogeneous porous media, *this volume.*

Zimmerman, R.W., S. Kumar, and G.S. Bodvarsson, 1991, Lubrication theory analysis of the permeability of rough-walled fractures, *Int. J. Rock. Mech. Min. Sci. & Geomech. Abstr., 28*, 325–331.

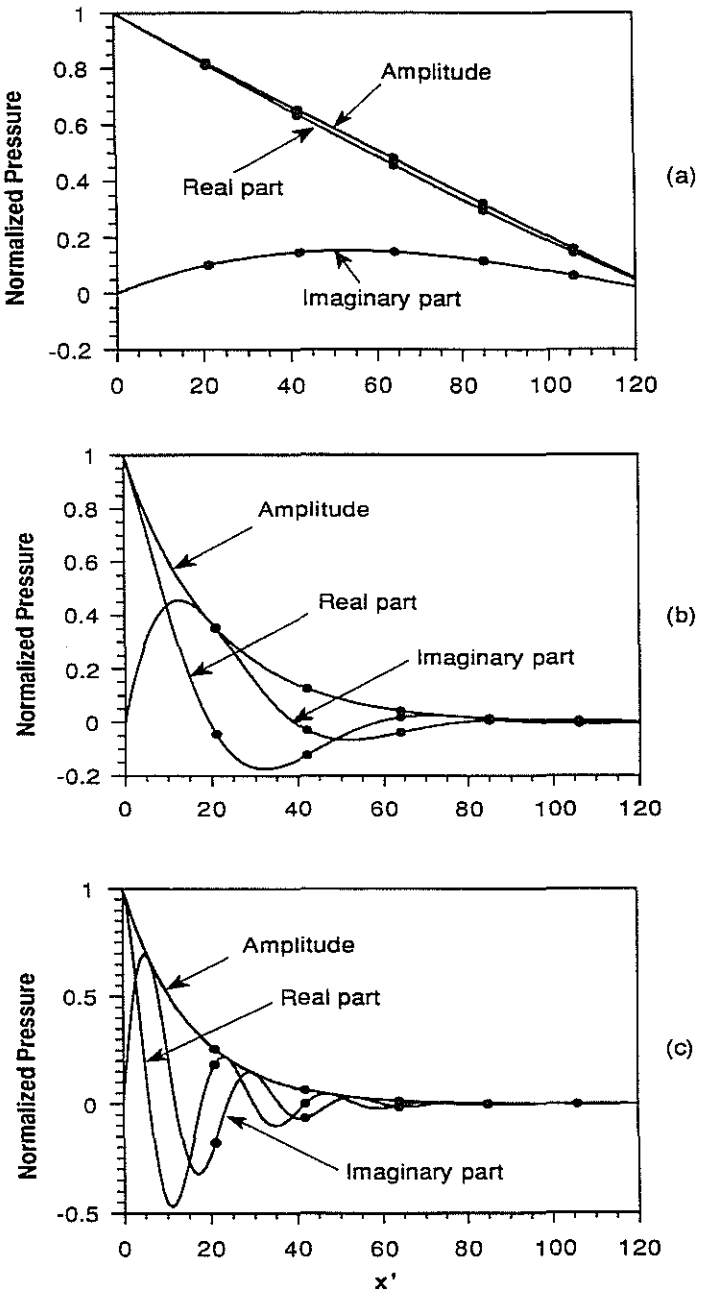

Figure 1: Comparison of finite-difference pressure decay curves along model length x' (dashed curves with dots) with 1-D analytic results (solid curves) for a homogeneous distribution at various frequencies. The frequencies are (a) 100 Hz, (b) 5000 Hz, and (c) 20000 Hz.

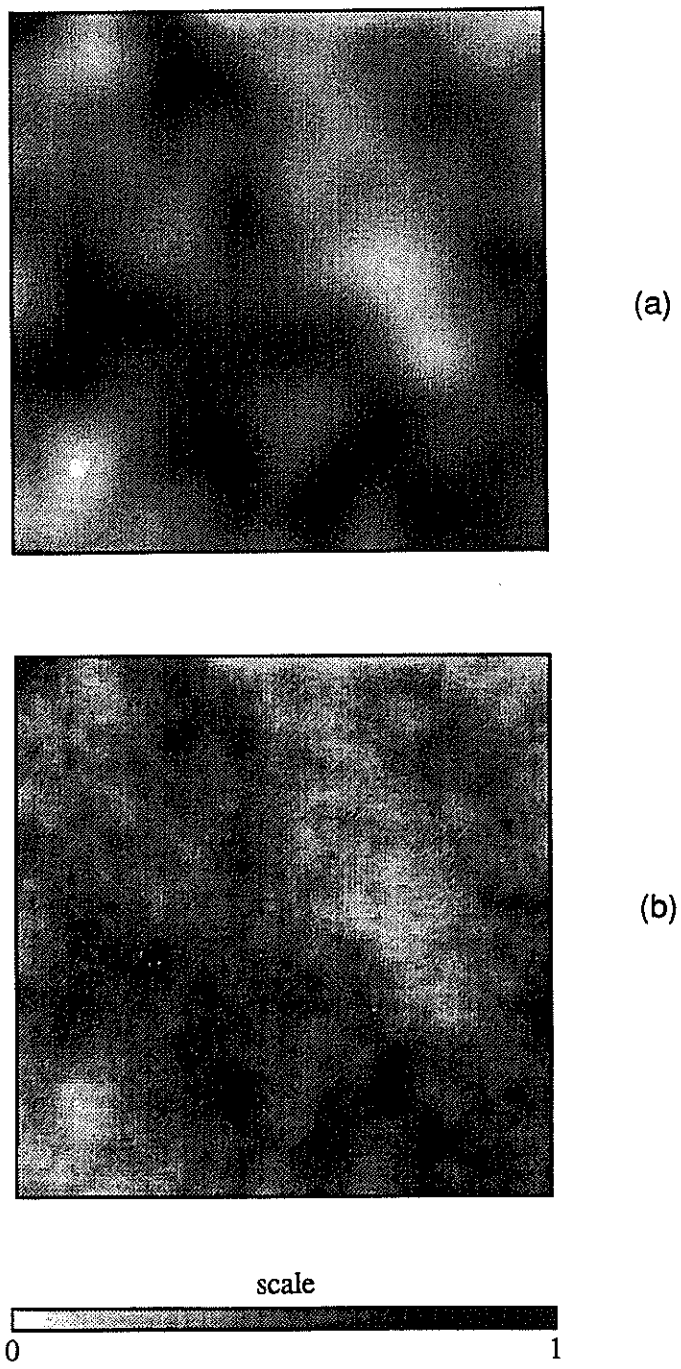

Figure 2: Two heterogeneous distributions generated by (a) Gaussian and (b) von-Karman correlation functions and the finite-difference modeling results [(c) and (d)] for the two distributions.

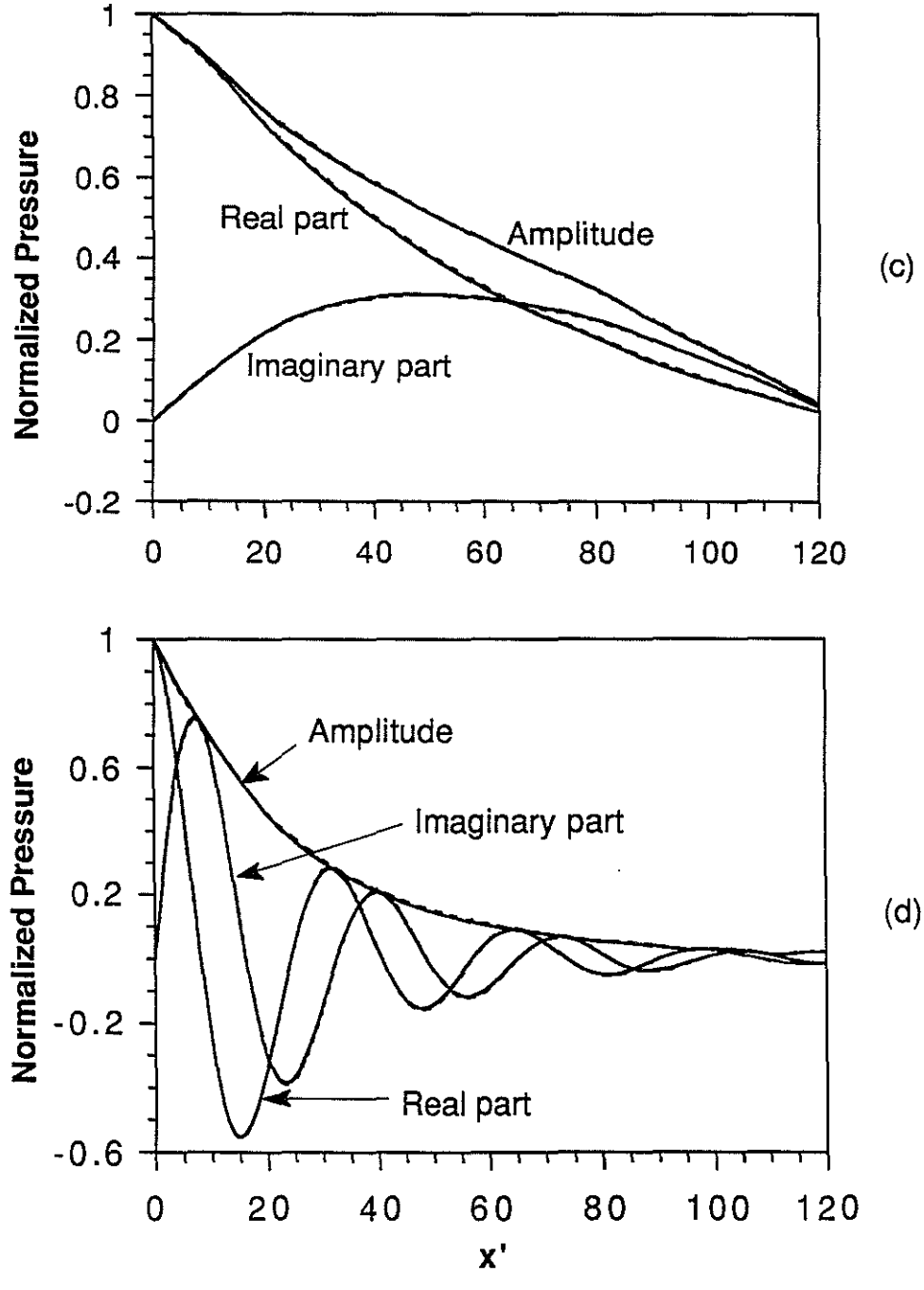

Figure 2: continued: Pressure decay curves for Gaussian (solid curves) and fractal (dashed curves) distributions at (c) 1000 Hz and (d) 30000 Hz.

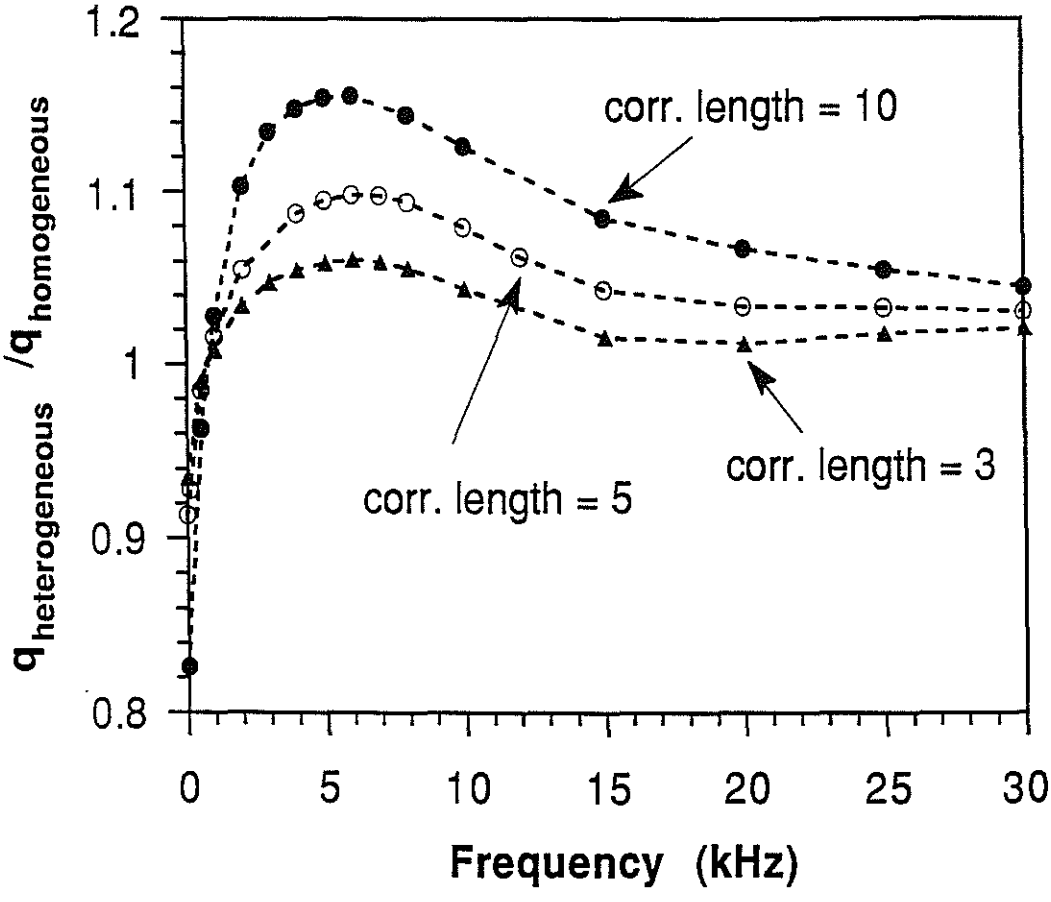

Figure 3: Fluid flow ratios through a heterogeneous and a homogeneous medium as functions of frequency.

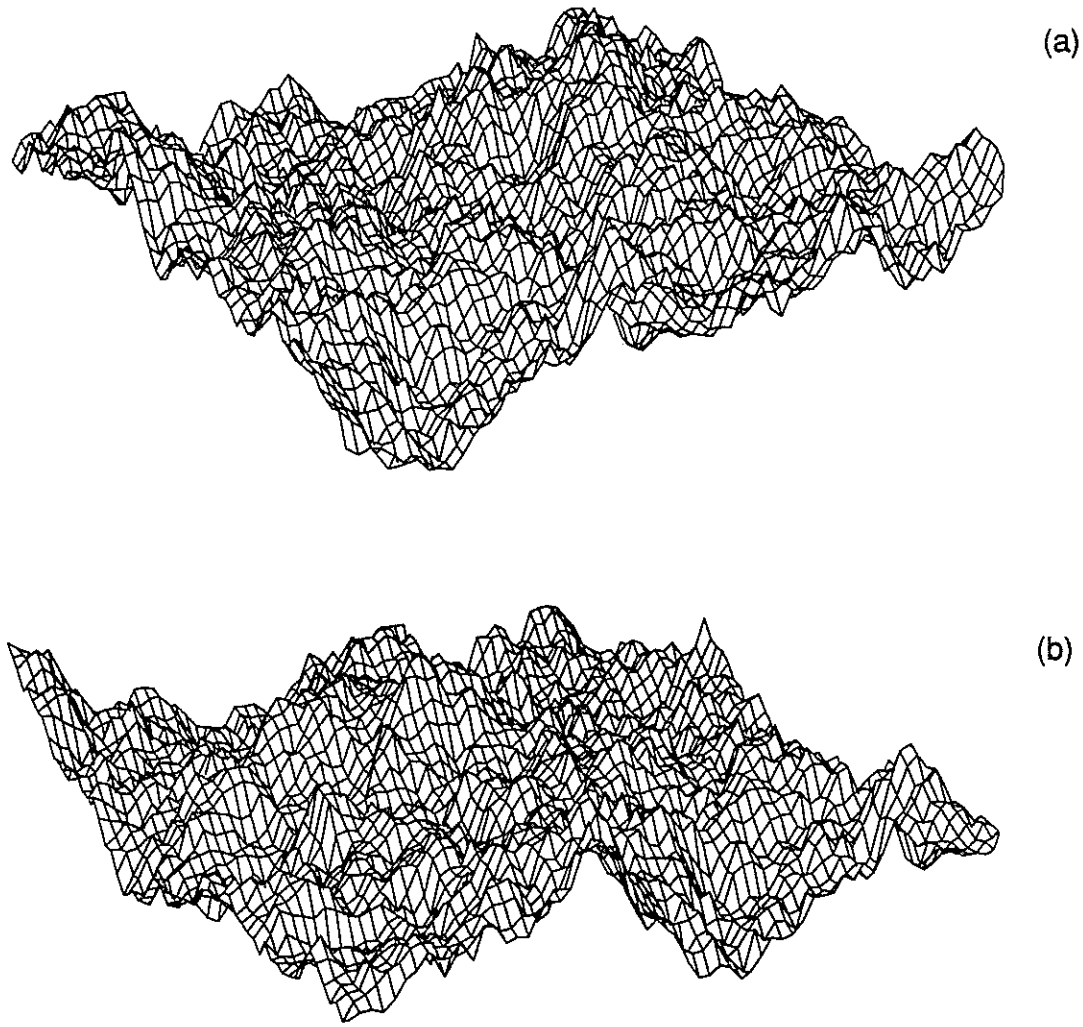

Figure 4: Rough surfaces representing the fracture walls. A fracture is formed by placing the two surfaces together (with one of them flipped over).

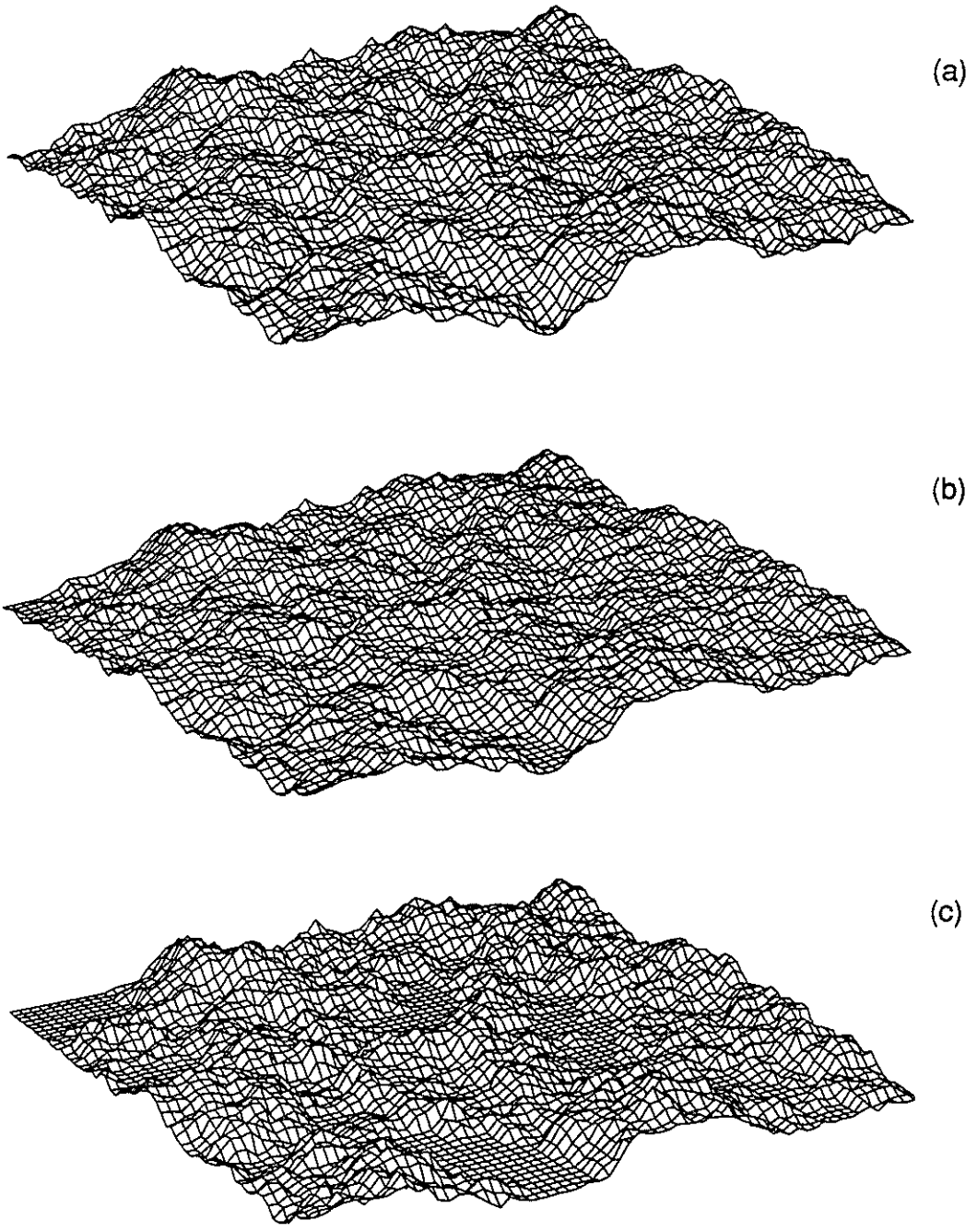

Figure 5: Examples of local aperture distribution formed using the two rough surfaces in Figure 4 with $d_m/\sigma = 10$ (a), 3 (b), and 1 (c).

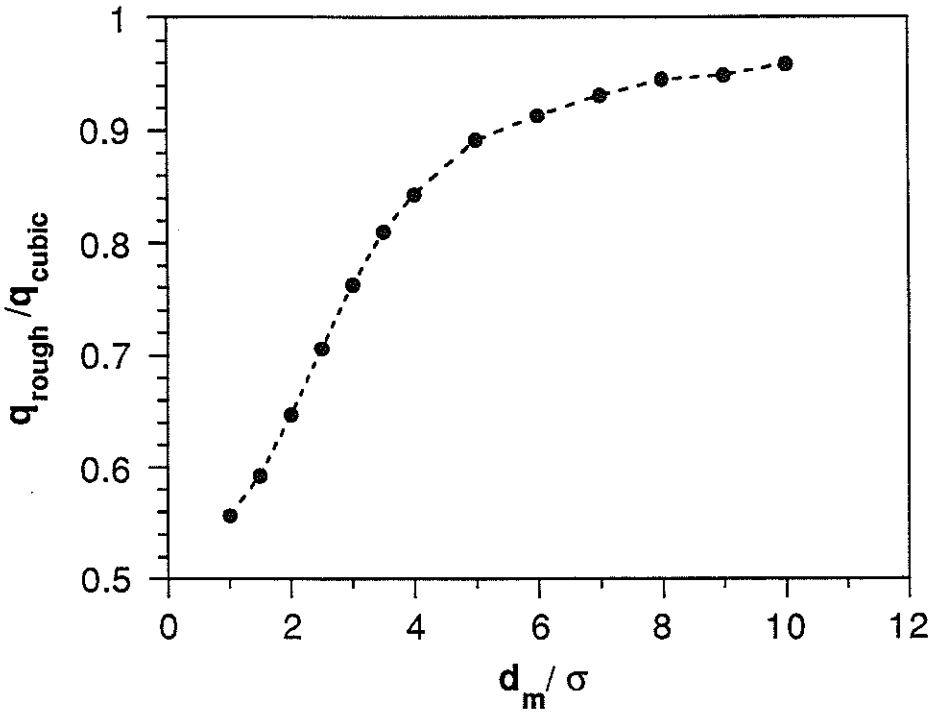

Figure 6: Comparison of fluid flow through a rough-walled fracture and a parallel plane wall fracture at zero frequency.

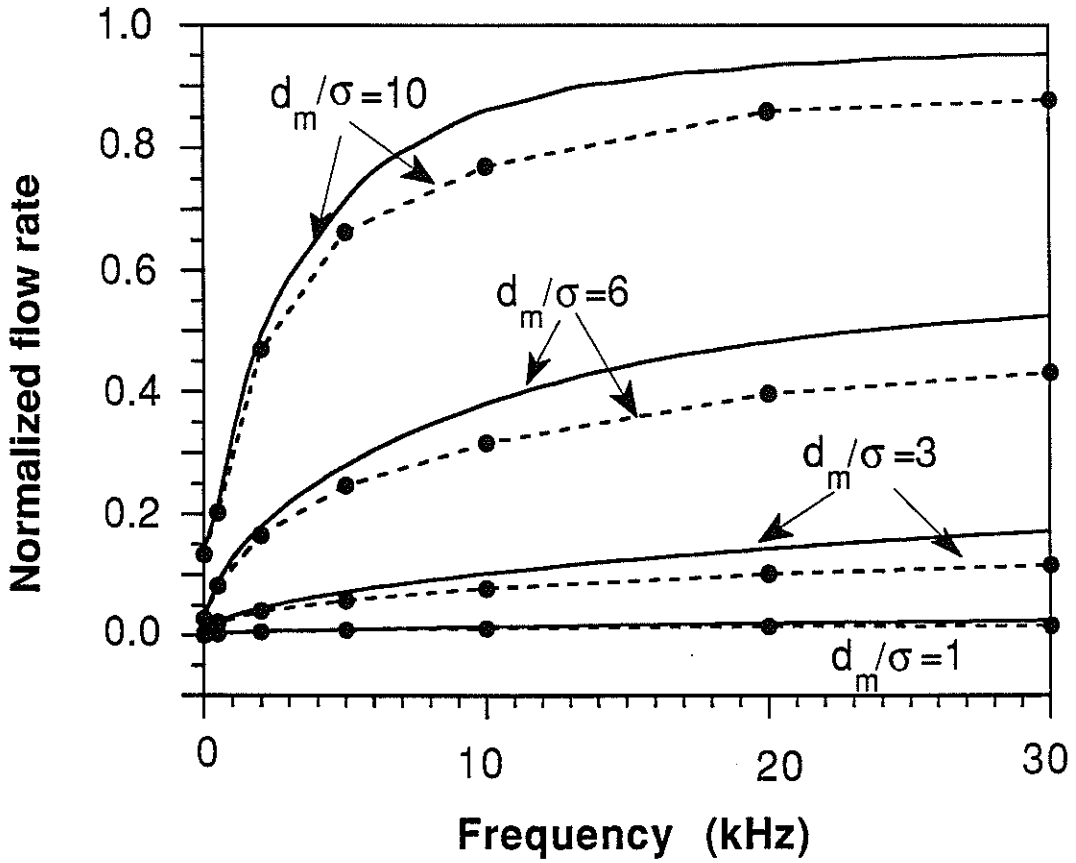

Figure 7: Fluid flow rate (scaled) versus frequency for rough-walled (dashed curves with dots) and plane (solid curves) fractures at various standard separations (d_m/σ).